Table 3 Density and bond bending found for ices IV, V and the new phase at 0.50 GPa and 260 K

Phase	ρ (g cm^{-1})	$\langle(\delta\theta)^2\rangle^{1/2}$
New phase	1.4365(1)	18.868
Ice IV	1.4361(1)	15.058
Ice V	1.4021(1)	19.067

$\langle(\delta\theta)^2\rangle^{1/2}$ is the r.m.s. of O···O···O bond angle deviations from the ideal tetrahedral angle of 109.5°, and ρ is density.

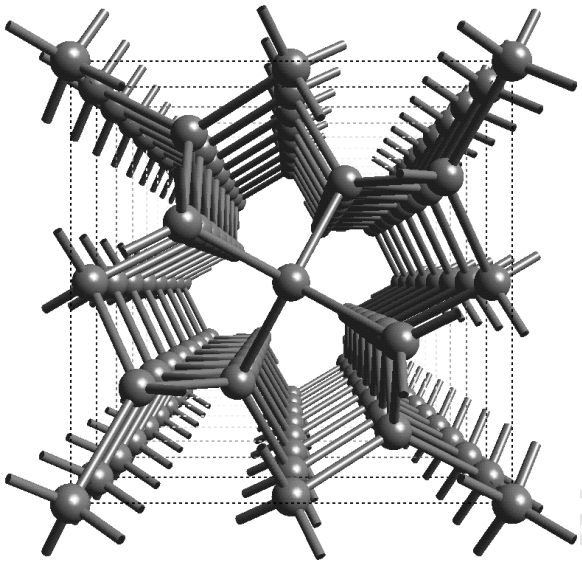

Figure 3 The oxygen framework of the new ice structure viewed down the *c*-axis.

The new phase is tetragonal, $a = 8.304$ Å, $c = 4.024$ Å, space group $I\bar{4}2d$. The unit cell comprises 12 water molecules, arranged to form a single-network tetrahedral structure. Fractional coordinates and refined bond lengths and angles are given in Tables 1 and 2 and the structure is shown in Fig. 3. The bond lengths are of the order expected for an ice in which the hydrogen atoms are positionally disordered: diffraction data give spatially averaged atomic positions which may differ from true local positions depending on the details of the disorder. Water molecules of type O(2) form zigzag chains which run parallel to the *c*-axis, and oscillate roughly parallel to either the *a*- or *b*-axis. These chains are then linked together by water molecules of type O(1), resulting in channels, roughly pentagonal in shape, running parallel to the *c*-axis. This configuration results in a density of 1.437 g cm^{-3}, which is greater than that of ice V at 1.402 g cm^{-3}, yet comparable with that of ice IV, 1.436 g cm^{-3}. For ice IV, the increase in density over ice V is achieved through a form of interpenetration, in which a hydrogen bond passes through a hexagonal ring of water molecules. For the new ice phase, no interpenetration of bonds is observed. Instead, the increase in density over ice V is achieved through additional bending of the hydrogen bonds (Table 3).

There can be no suggestion that this new phase is ice IV. Although the structure of ice IV in the literature was determined from samples recovered at low temperature to ambient pressure[7], in other measurements we have also formed and refined the structure of ice IV under pressure[5], and can thus confirm that the structure of ice IV under these pressure and temperature conditions is that proposed by Engelhardt and Kamb[7].

The designation of phases I through to XI now seems to be accepted. Although the label of ice XII has already been used by Sirota and Bizhigitov[8] for a low-temperature phase in the pressure range of ice VI and VIII, the evidence for this phase is from relative volume changes observed in piston-in-cylinder cell measurements, with no direct structural technique having been used in its investigation. Despite the efforts of several groups, the phase suggested by Sirota and Bizhigitov[8] has never been confirmed. We therefore provisionally propose that this new phase reported here be named ice XII. (It seems sensible to follow the generally accepted view that Roman numerals be used only for experimentally established crystalline phases, with crystallographic or at least spectroscopic evidence required to fulfil the criterion of 'experimental evidence'.)

The new picture that emerges is of two disordered phases of ice, ices IV and XII, that are very similar in density yet are topologically very different. Both phases are likely to be metastable with respect to ice V, but have somewhat higher density. The existence of 5- and 7-fold rings is interesting, although not unexpected: such local geometries are entirely consistent with the roughly tetrahedral geometry of the intermolecular interaction, and are found in some other ice structures (for example, ices III and V). The enhanced richness of the ice phase diagram in the medium pressure range is another demonstration of the versatility of the water molecule in building a variety of fully hydrogen-bonded structures. The seemingly delicate balance of enthalpic and entropic contributions to the total energy will allow us to test critically the viability of water potential functions used widely in computer simulations of chemical and biomolecular systems. The water system also seems to be an excellent candidate for general studies of metastability, including both thermodynamic and kinetic aspects of phase formation. □

Received 26 August; accepted 27 October 1997.

1. Hobbs, P. V. *Ice Physics* (Clarendon, Oxford, 1974).
2. Kamb, B., Prakash, A. & Knobler, C. Structure of ice V. *Acta Cryst.* **22,** 706–715 (1967).
3. Bridgman, P. W. The *P–V–T* relations of the liquid, and the phase diagram of heavy water. *J. Chem. Phys.* **3,** 597–605 (1935).
4. Engelhardt, H. & Whalley, E. Ice IV. *J. Chem. Phys.* **56,** 2678–2684 (1972).
5. Lobban, C. *Neutron Diffraction Studies of Ices.* Thesis, Univ. London (1998).
6. Larsen, A. C. & Von Dreele, R. B. *GSAS—General Structure Analysis System.* (University of California, 1985).
7. Engelhardt, H. & Kamb, B. Structure of ice IV, a metastable high-pressure phase. *J. Chem. Phys.* **75,** 5887–5899 (1981).
8. Bizhigitov, T. B. & Sirota, N. N. Low-temperature modification of high-pressure ice. *JETP Lett.* **44,** 417–419 (1986).

Acknowledgements. We thank CCLRC and the Institut Laue-Langevin for access to the ISIS and ILL neutron facilities respectively, including generous allocation of the director's discretionary time which was crucial in obtaining data of quality adequate for the structure refinement. We thank also J. Dreyer and T. Cooper (ISIS) and L. Melesi (ILL) for their extensive efforts on the high-pressure equipment.

Correspondence and requests for materials should be addressed to either J.L.F. (e-mail: j.finney@ucl.ac.uk) or W.F.K. (e-mail: kuhs@silly.uni-mki.gwdg.de).

Silicate regulation of new production in the equatorial Pacific upwelling

Richard C. Dugdale & Frances P. Wilkerson

Romberg Tiburon Centers, San Francisco State University, PO Box 855, Tiburon, California 94920, USA

Surface waters of the eastern equatorial Pacific Ocean present the enigma of apparently high plant-nutrient concentrations but low phytoplankton biomass and productivity[1]. One explanation for this 'high-nitrate, low-chlorophyll' (HNLC) phenomenon has been that growth is limited by iron availability[2,3]. Here we use field data and a simple silicon-cycle model[4] to investigate the HNLC condition for the upwelling zone of this ocean region. Measured silicate concentrations in surface waters are low and largely invariant with time, and set the upper limit on the total possible biological utilization of dissolved inorganic carbon.

Chemical and biological data from surface waters indicate that diatoms—silica-shelled phytoplankton—carry out all the 'new production' (nitrate uptake)[5]. Smaller phytoplankton (picoplankton) accomplish most of the total primary production, largely fuelled by nitrogen regenerated in reduced forms as a result of grazing by zooplankton. The model predicts values of new and export production (the production exported to below the euphotic zone) that compare well with measured values[6]. New and export production are in balance for biogenic silica, whereas new production exceeds export for nitrogen. The HNLC condition in the upwelling zone can therefore be understood to be due to a chemostat-like regulation of nitrate uptake by upwelled silicate supply to diatoms: 'low-silicate HNLC'. These results are not inconsistent with observations of iron-fertilized diatom growth during *in situ* experiments in 'low-iron HNLC' waters outside this upwelling zone[2,3], but reflect the role of different supply rates of iron and silicate in determining the nature of the HNLC condition.

The equatorial upwelling zone (EUZ) of the eastern equatorial Pacific Ocean—where biological drawdown of CO_2 is low due to weak primary production—is a net source of CO_2 to the atmosphere. The EUZ is characterized by relatively continuous upwelling driven by the trade winds; this has led to it being considered as a chemostat culture system[7], in which nutrient supply regulates phytoplankton growth. Modelling and field data show[4] that open-ocean upwelling systems tend to become silicate-limited through differential export of Si compared to N. Zooplankton grazing on diatoms leads to much greater regeneration of N than silicate ($Si(OH)_4^{2-}$) in euphotic zone waters, so that the disappearance ratios of NO_3^-:$Si(OH)_4^{2-}$ are <1 (as low as 0.25 in Southern Ocean surface waters[8]). These systems are eventually driven into silicate limitation by the rate of supply of silicate. $Si(OH)_4^{2-}$ stabilizes at a regulating concentration below that of NO_3^- through a feedback process that sets up the steady-state balance between nutrient supply rate and population size (nutrient demand).

The ratio of $Si(OH)_4^{2-}$:NO_3^- in equatorial upwelled source waters is usually less than the 1:1 ratio[9] realized by diatoms, and studies have shown[10] $Si(OH)_4^{2-}$ to be transported into the equatorial upwelling zone at a rate of 0.8 times that of NO_3^-. The special role of diatom production ($Si(OH)_4^{2-}$ drawdown) in the equatorial drawdown of total CO_2 (ΣCO_2) can be seen from the similarity in slopes of equatorial ΣCO_2 versus $Si(OH)_4^{2-}$ and NO_3^- (Fig. 1a, b). Using the approach of Broecker and Peng[11], these regressions show this relationship to be true for both deeper samples, which tend to have a slope of near Redfield (C/N = 6.6), and for near-surface data where ΣCO_2 has been reduced by exchange with the atmosphere[11]. The higher intercepts in Fig. 1b show that the maximum ΣCO_2 drawdown due to biological production is a function of the ΣCO_2 versus $Si(OH)_4^{2-}$ rather than NO_3^- relationship; NO_3^- uptake appears to cease when $Si(OH)_4^{2-}$ falls to some low concentration ($\sim$2 mmol m^{-3}; Fig. 1c). The NO_3^- versus $Si(OH)_4^{2-}$ slope for the

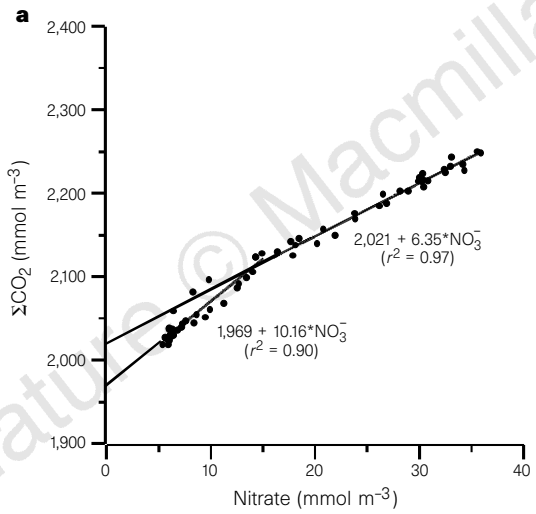

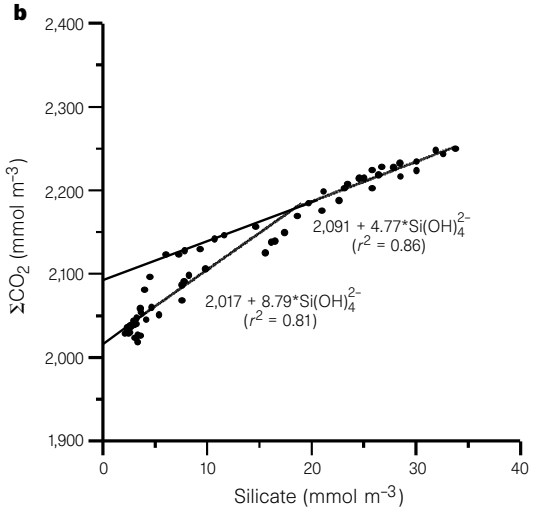

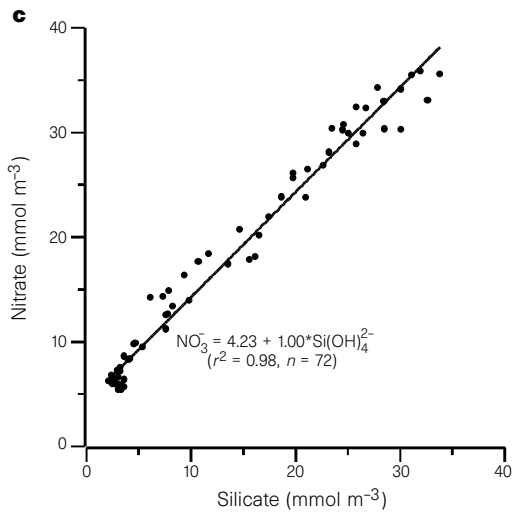

Figure 1 Data from the upper 200 m of water, at 140° W, 1° N to 1° S measured during JGOFS EqPac autumn 1992 TT011 cruise (data available at http://www1. whoi. edu/jgofs.html). Slopes fitted by linear regression. **a** and **b**, ΣCO_2 (total dissolved inorganic carbon concentration[26]) versus nutrient concentration; **a**, NO_3^-; **b**, $Si(OH)_4^{2-}$. **c**, NO_3^- versus $Si(OH)_4^{2-}$.

same data (Fig. 1c) is 1.00 ($r^2 = 0.98$), indicating that NO_3^- is taken up exclusively by the diatom population as the 1:1 slope of disappearance is identical to the biomass ratio of $Si(OH)_4^{2-}$ and N of diatoms[12]. The N requirement of the diatoms is apparently met fully by NO_3^- uptake, implying an *f* ratio (of new to total production) for that population of 1. However, the measured *f* ratio for the entire autotrophic community is low (0.17 (ref. 13) and 0.1–0.13 (ref. 14)), indicating that essentially all of the non-diatom production is based on recycled N, such as NH_4^+ arising from grazing on diatoms that is taken up exclusively by the smaller phytoplankton (picoplankton) whose production is entirely regenerated in a similar way to that described for the Benguela upwelling system[15]. This results in a tightly coupled loop that strongly conserves N and forces the community *f* ratio to a low value.

The silicate pump model[4] was initiated for the EUZ after adding a picoplankton loop (Fig. 2) with no NH_4^+ recycled to the diatoms. Si dissolution rates were assumed to be negligible as there are no contemporary observations and the only upwelling value (from coastal upwelling) is 10% (ref. 16). Parameters used to initiate the model were taken from JGOFS EqPac autumn 1992 (TT011) data[6] except for sinking and grazing parameters (faecal pellet production, FPP = 0.3, growth efficiency GEFF = 0.3; refs 4, 17) and upwelling rate[4] (1 m d^{-1}). The latter value falls within the range of 0.8 to 1.5 m d^{-1} obtained at 140° W, autumn 1992[18]. Nutrient concentrations used were from 100 m for the source concentrations (NO_3^- = 10.95 mmol m^{-3}, $Si(OH)_4^{2-}$ = 5.67 mmol m^{-3}) and from 10 m for the euphotic zone (NO_3^- = 5.93 mmol m^{-3}, $Si(OH)_4^{2-}$ = 2.68 mmol m^{-3}). Diatom biomass as biogenic silicon, BSi, was calculated as 0.043 mmol m^{-3} from an estimate of the proportion of total chlorophyll that was diatom chlorophyll (chl; 12%)[19], converted to particulate nitrogen (PON) and BSi using 1 μg l^{-1} chl = 1 mmol m^{-3} PON (ref. 4) and 1:1 PON:BSi, as no BSi measurements are available. This result agrees well with a less direct estimate (0.03 mmol m^{-3}) obtained using diatom carbon calculated from size[20]. The net upwelling supply rates of $Si(OH)_4^{2-}$ and NO_3^- were calculated as the product of upwelling rate and the gradient from source to mixed-layer nutrient concentrations[4], and silicate supply rate was taken as the new production rate, as it is the lower of the two. Using a 1:1 ratio of $Si(OH)_4^{2-}$:NO_3^- uptake, both rates are set to 2.36 mmol m^{-2} d^{-1}, which compares well with the ^{15}N measured value[14] of 2.80 mmol m^{-2} d^{-1}. The model results (Table 1) show all grazed BSi to be assigned to faecal pellet production, compared to 30% for grazed N, and losses due to sinking and upwelling dilution are insignificant compared to grazing. An important consequence of the model structure is that export production of Si equals new $Si(OH)_4^{2-}$ production, whereas export production of N is much less than new N production. Nitrogen export, calculated as 0.76 mmol m^{-2} d^{-1}, falls within measured values[21] (0.3–1.06 m^{-2} d^{-1}). Total production (915.5 mg C m^{-2} d^{-1}) is comparable to the EqPac autumn 1992 value[22] of 1,500 mg C m^{-2} d^{-1}, greater than would be predicted from the low levels of NO_3^- uptake. Grazing on diatoms supplies a new source of N as NH_4^+ to the picoplankton, which is regenerated ($f = 0.1$) in the microbial loop. The model community value of $f = 0.2$ (new/total production) is in good agreement with the measured value[14] of 0.23.

Euphotic-layer $Si(OH)_4^{2-}$ concentrations measured during three cruises (WEC 88, EqPac spring 1992 and EqPac autumn 1992) to the EUZ showed little variability (2.65–2.77 mmol m^{-3}) compared to the higher and more variable NO_3^- concentrations (2.76–5.93 mmol m^{-3}). These observations are consistent with chemostat conditions, in which the relative concentrations of the required nutrients in the feed medium determine which nutrient will be limiting (silicate in this case), and the loss rates set the growth rate of the organism. Regulation of the diatom growth rate, and consequently of the new production system, requires that the growth rate and the limiting substrate concentration define a point on an operating curve (typically a Michaelis–Menten relationship). To identify the operating point for EUZ an estimate of the specific silicate uptake ($V_{Si(OH)_4^{2-}} = 0.82\ d^{-1}$) was obtained using ^{15}N data[14], assuming nitrate uptake ($\rho_{NO_3^-}$, mmol l^{-1} d^{-1}) = silicate uptake ($\rho_{Si(OH)_4^{2-}}$, mmol l^{-1} d^{-1}) and dividing $\rho_{Si(OH)_4^{2-}}$ by BSi (0.043 mmol m^{-3}). The steady-state silicate concentration for this value of $V_{Si(OH)_4^{2-}}$ calculated with a half-saturation constant $K_S = 3$ mmol m^{-3} and $V_{max} = 1.92\ d^{-1}$ is 2.24 mmol m^{-3}, in good agreement with the silicate range observed above (2.65–2.77 mmol m^{-3}). The $V_{Si(OH)_4^{2-}}$ value compares well with the directly measured diatom growth rate[19] ($\mu = 0.67\ d^{-1}$) and both fall close to the Michaelis–Menten curve. The diatom population is regulating at about half the maximal uptake and with a substrate concentration near K_S. The ability of the diatom population to achieve steady-state growth rates of ~1 d^{-1}, sufficient to offset the sum of the loss rates, shows that limitation by other factors such as iron need not be invoked. Oceanic diatoms can reach maximal growth rates of 1 d^{-1} with low iron[23]. The supply of new iron in the upwelling water[22] is

Table 1 Model results of N and Si partitioning and productivity

	mmol N m^{-2} d^{-1}	mmol Si m^{-2} d^{-1}	mg C m^{-2} d^{-1}
Inputs			
Upwelling supply (NO_3^-, $Si(OH)_4^{2-}$)	3.97	2.36	
Diatom uptake rate (NO_3^-, $Si(OH)_4^{2-}$)	2.36	2.36	
Outputs			
Grazing rate	2.29	2.29	
Faecal pellet production rate	0.69	2.29	
Sinking rate	0.034	0.034	
Upwelling dilution rate	0.034	0.034	
Export production*	0.76	2.36	
Predation rate	0.69	0	
New production (that is diatom production)	2.36	2.36	186.91
Regenerated production (that is, picoplankton production)	9.20	0	728.64
NH_4^+ supplied from grazing on diatoms	0.92		
NH_4 supplied from micrograzers	8.28		
Total production†	11.56		915.55

* Calculated as faecal production rate and sinking rate and upwelling dilution rate.
† Calculated as new production and regenerated production.

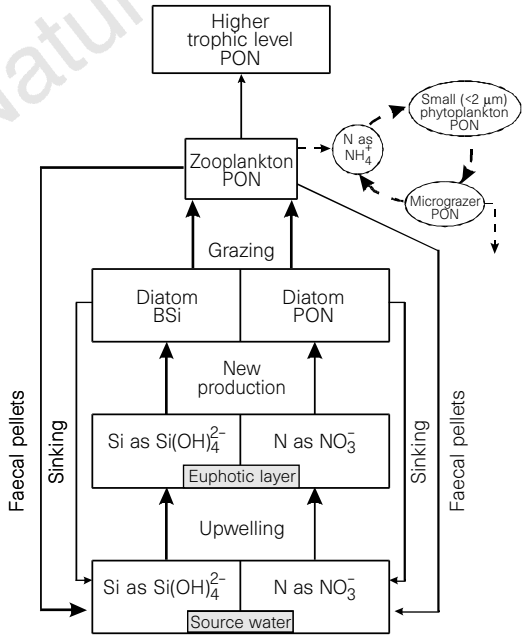

Figure 2 Silicate pump model[4] modified to include a picoplankton/micrograzer loop. PON, particulate organic nitrogen.

apparently sufficient to allow diatom growth at the levels required for steady state.

Additions of iron in the EUZ may change the operating point of the silicate uptake curve, for example, by increasing the initial slope. The transient effect would be a small net increase in diatom growth rate over grazing rate or increase in biomass, as has been observed[24] after 4–5 days. A longer-term effect of this change in operating point would be to decrease the euphotic-layer silicate concentration, resulting in an increase of the source to euphotic-zone silicate gradient, and an increase in new production. This gradient increase is always relatively small and therefore any increase in new production minimal, because the concentration of euphotic-layer silicate in the EUZ is already close to or at K_S concentrations. Although our results appear to conflict with those of the IronEx open-ocean experiments in which clear responses to iron additions were observed[2,3], the contradictions can be resolved by recognizing the important differences in conditions of JGOFS EqPac and IronEx studies. In the EUZ, new iron is fed into the surface waters, along with new $Si(OH)_4^{2-}$ and NO_3^- fuelling the diatom productivity observed. The IronEx experiments were conducted outside the EUZ in the South Equatorial Current, where the atmosphere is the only source of new iron and the area is prone to chronic iron limitation. Although $Si(OH)_4^{2-}$ values were not reported for IronEx, they would be lower than NO_3^-, as the source water for this current arises from the low-silicate HNLC region offshore from Peru[4]. Because the response of NO_3^- uptake in IronEx II was seen exclusively in the larger (>5 μm) algal size-class (diatoms)[3], our results suggest that even with iron enrichment, the maximum drawdown of CO_2 in this region would eventually be limited by silicate availability.

To increase CO_2 drawdown in the EUZ and reach coastal upwelling values of new production, an order-of-magnitude increase in upwelling rate combined with an increase in source silicate concentration would be necessary[4]. The ^{15}N measured new production[14] during the EqPac autumn 1992 study was 0.03 mmol N m^{-3} d^{-1}, about two orders of magnitude below the range of new production for coastal upwelling[25], 0.4–4.2 mmol N m^{-3} d^{-1}. As the euphotic-zone silicate concentration is constant (a result of silicate regulation), the source concentration of silicate alone determines the vertical gradient of this species if no changes in mixed-layer depth occur. Under these conditions, the source silicate concentration and the upwelling rate are the remaining variables determining the new production rate. By elevating both source silicate concentration (for example, from 5.67 to 20 mmol m^{-3}) and the upwelling rate, w (from 1 to 10 m d^{-1}), the new production would reach 1.73 mmol m^{-3} d^{-1} (coastal upwelling levels[25]). Neither variable alone can achieve such rates (that is, $Si(OH)_4^{2-} = 20$ mmol m^{-3}, $w = 1$ m d^{-1} gives $\rho_{NO_3^-} = 0.17$ mmol m^{-3} d^{-1}, and increasing w to 10 m d^{-1} with $Si(OH)_4^{2-} = 5.67$ mmol m^{-3} d^{-1} gives $\rho_{NO_3^-} = 0.3$ mmol m^{-3} d^{-1}).

The EUZ has characteristics that are operationally analogous to chemostat culture systems, specifically (1) constant limiting nutrient concentrations with variable non-limiting concentrations, (2) growth rates as a function of loss rates; and (3) an operating point on a known nutrient/growth-rate curve. The "excess NO_3^-" previously observed[1] that led to the classification of the eastern equatorial Pacific as HNLC can now be understood as the consequence of silicate limitation, because new N is taken up only by diatoms. Potential new production based on nitrate concentration is not realized. This area, like some other HNLC areas described previously[4], should be classified as low-silicate HNLC to avoid the impression that all 'major nutrient' concentrations are sufficiently high to support new production. The results obtained in the IronEx locations of the eastern equatorial Pacific should not be extrapolated to the EUZ, which has a source of new iron and in which the potential for increased new and export production, by whatever means, is very small. □

Received 28 February; accepted 21 October 1997.

1. Barber, R. T. & Chavez, F. P. Regulation of primary productivity rate in the equatorial Pacific. *Limnol. Oceanogr.* **36,** 1803–1815 (1991).
2. Martin, J. H. *et al.* Testing the iron hypothesis in ecosystems of the equatorial Pacific Ocean. *Nature* **371,** 123–129 (1994).
3. Coale, K. H. *et al.* A massive phytoplankton bloom induced by an ecosystem-scale iron fertilization experiment in the equatorial Pacific Ocean. *Nature* **383,** 495–501 (1996).
4. Dugdale, R. C., Wilkerson, F. P. & Minas, H. J. The role of a silicate pump in driving new production. *Deep-Sea Res. I* **42,** 697–719 (1995).
5. Dugdale, R. C. & Goering, J. J. Uptake of new and regenerated forms of nitrogen in primary productivity. *Limnol. Oceanogr.* **12,** 196–207 (1967).
6. Murray, J. W., Johnson, E. & Garside, C. A U.S. JGOFS Process Study in the equatorial Pacific (EqPac): Introduction. *Deep-Sea Res. II* **42,** 275–293 (1995).
7. Frost, B. W. & Franzen, N. C. Grazing and iron limitation in the control of phytoplankton stock and nutrient concentration: a chemostat analogue of the Pacific equatorial upwelling zone. *Mar. Ecol. Prog. Ser.* **83,** 291–303 (1992).
8. Minas, H. J. & Minas, M. Net community production in "High Nutrient-Low Chlorophyll" waters of the tropical and Antarctic Oceans: grazing versus iron hypothesis. *Oceanol. Acta* **15,** 145–162 (1992).
9. Wilkerson, F. P. & Dugdale, R. C. Silicate versus nitrate limitation in the equatorial Pacific estimated from satellite-derived sea-surface temperatures. *Adv. Space Res.* **18,** 81–89 (1996).
10. Ku, T.-L., Luo, S., Kusakabe, M. & Bishop, J. K. B. ^{228}Ra-derived nutrient budgets in the upper equatorial Pacific and the role of "new" silicate in limiting productivity. *Deep-Sea Res. II* **42,** 479–497 (1995).
11. Broecker, W. S. & Peng, T.-H. *Tracers in the Sea* (Eldigio, New York, 1982).
12. Brzezinkski, M. A. The Si:C:N ratio of marine diatoms: interspecific variability and the effect of some environmental variables. *J. Phycol.* **21,** 347–357 (1985).
13. Dugdale, R. C., Wilkerson, F. P., Barber, R. T. & Chavez, F. P. Estimating new production in the equatorial Pacific Ocean at 150° W. *J. Geophys. Res.* **97,** 681–686 (1992).
14. McCarthy, J. J., Garside, C., Nevins, J. L. & Barber, R. T. New production along 140° W in the equatorial Pacific during and following the 1992 El Niño event. *Deep-Sea Res. II* **43,** 1065–1093 (1996).
15. Probyn, T. A. The inorganic nitrogen nutrition of phytoplankton in the southern Benguela: New production, phytoplankton size, and implications for pelagic food webs. *S. Afr. J. Sci.* **12,** 411–420 (1992).
16. Nelson, D. M., Goering, J. J. & Boisseau, D. W. in *Coastal Upwelling* Vol. 1 (ed. Richards, F. A.) (Am. Geophys. Un., Washington DC, 1981).
17. Michaels, A. F. & Silver, M. W. Primary production, sinking fluxes and the microbial food web. *Deep-Sea Res.* **35,** 473–490 (1988).
18. Wanninkhof, R. A. *et al.* Seasonal and lateral variations in carbon chemistry of surface water in the eastern equatorial Pacific during 1992. *Deep-Sea Res. II* **42,** 387–409 (1995).
19. Bidigare, R. R. & Ondrusek, M. E. Spatial and temporal variability of phytoplankton pigment distributions in the central equatorial Pacific Ocean. *Deep-Sea Res. II* **43,** 809–833 (1996).
20. Kaczmarska, I. & Fryxell, G. A. Microphytoplankton of the equatorial Pacific: 140° W meridional transect during the 1992 El Niño. *Deep-Sea Res. II* **42,** 535–558 (1995).
21. Buesseler, K. O., Andrews, J. A., Hartman, M. C., Belastock, R. & Chai, F. Regional estimate of the export flux of particulate organic carbon derived from Thorium-234 during the JGOFS EqPac program. *Deep-Sea Res. II* **42,** 777–804 (1995).
22. Barber, R. T. *et al.* Primary productivity and its regulation in the equatorial Pacific during and following the 1991–1992 El Niño. *Deep-Sea Res. II* **43,** 933–969 (1996).
23. Sunda, W. G., Swift, D. G. & Huntsman, S. A. Low iron requirement for growth in oceanic phytoplankton. *Nature* **351,** 55–57 (1991).
24. Fitzwater, S. E., Coale, K. H., Gordon, R. M., Johnson, K. S. & Ondrusek, M. E. Iron deficiency and phytoplankton growth in the equatorial Pacific. *Deep-Sea Res. II* **43,** 995–1015 (1996).
25. Dugdale, R. C. & Wilkerson, F. P. in *Primary Productivity and Biogeochemical Cycles in the Sea* (eds Falkowski, P. G. & Woodhead, A. D.) 107–122 (Plenum, New York, 1992).
26. Archer, D. E. *et al.* Daily, seasonal and interannual variability of sea surface carbon and nutrient concentrations in the equatorial Pacific Ocean. *Deep-Sea Res. II* **43,** 779–809 (1996).

Acknowledgements. This work was supported by the US NSF and Region Provence Alpes Maritimes Cooperative Agreement.

Correspondence and requests for materials should be addressed to R.C.D. (e-mail: rdugdale@sfsu.edu).

Three-dimensional glacial flow and surface elevation measured with radar interferometry

Johan J. Mohr, Niels Reeh & Søren N. Madsen

Danish Center for Remote Sensing, Department of Electromagnetic Systems, Technical University of Denmark, DK-2800 Lyngby, Denmark

Outlet glaciers—which serve to drain ice from ice sheets—seem to be dynamically less stable in North Greenland than in South Greenland[1–3]. Storstrømmen, a large outlet glacier in northeastern Greenland which surged between 1978 and 1984 (ref. 2), has been well studied. In general, neither glacier surge mechanisms nor the geographical distribution of the surges are well known. Conventional satellite radar interferometry can provide large-scale topography models with high resolution[4], and can measure